SLAC-PUB-11428

To be submitted to ApJ

Evidence for a Canonical GRB Afterglow Light Curve in the *Swift*/XRT Data

J. A. Nousek[1], C. Kouveliotou[2], D. Grupe[1], K. Page[3], J. Granot[4], E. Ramirez-Ruiz[5,6], S. K. Patel[7,2], D. N. Burrows[1], V. Mangano[8], S. Barthelmy[12], A. P. Beardmore[3], S. Campana[9], M. Capalbi[10], G. Chincarini[9,11], G. Cusumano[8], A. D. Falcone[1], N. Gehrels[12], P. Giommi[10], M. Goad[3], O. Godet[3], C. Hurkett[3], J. A. Kennea[1], A. Moretti[9], P. O'Brien[3], J. Osborne[3], P. Romano[9], G. Tagliaferri[9], A. Wells[3]

ABSTRACT

We present new observations of the early X-ray afterglows of the first 27 gamma-ray bursts (GRBs) detected with the *Swift* X-ray Telescope (XRT). The early X-ray afterglows show a canonical behavior, where the light curve broadly consists of three distinct power law segments: (i) an initial very steep decay ($\propto t^{-\alpha}$ with $3 \lesssim \alpha_1 \lesssim 5$) , followed by (ii) a very shallow decay ($0.2 \lesssim \alpha_2 \lesssim 0.8$), and finally (iii) a somewhat steeper decay ($1 \lesssim \alpha_3 \lesssim 1.5$). These power law

[1]Department of Astronomy & Astrophysics, Pennsylvania State University, University Park, PA 16802, USA

[2]NASA/Marshall Space Flight Center, National Space Science Technology Center, XD-12, 320 Sparkman Drive, Huntsville, AL 35805, USA.

[3]Department of Physics and Astronomy, University of Leicester, Leicester, UK

[4]Kavli Institute for Particle Astrophysics and Cosmology, Stanford University, P.O. Box 20450, MS 29, Stanford, CA 94309.

[5]Institute for Advanced Study, Einstein Drive, Princeton, NJ 08540, USA.

[6]Chandra Fellow.

[7]IPA with NASA/MSFC through Universities Space Research Association

[8]INAF- Istituto di Fisica Spazialee Fisica Cosmica sezione di Palermo, Palermo, Italy

[9]INAF – Osservatorio Astronomico di Brera, Merate, Italy

[10]ASI Science Data Center, Frascati, Italy

[11]Università degli studi di Milano-Bicocca, Dipartimento di Fisica, Milan, Italy

[12]NASA/Goddard Space Flight Center, Greenbelt, MD

Work supported in part by Department of Energy contract DE-AC02-76SF00515

segments are separated by two corresponding break times, 300 s $\lesssim t_{\rm break,1} \lesssim$ 500 s and 10^3 s $\lesssim t_{\rm break,2} \lesssim 10^4$ s. On top of this canonical behavior of the early X-ray light curve, many events have superimposed X-ray flares, which are most likely caused by internal shocks due to long lasting sporadic activity of the central engine, up to several hours after the GRB. We find that the initial steep decay is consistent with it being the tail of the prompt emission, from photons that are radiated at large angles relative to our line of sight. The first break in the light curve ($t_{\rm break,1}$) takes place when the forward shock emission becomes dominant, with the intermediate shallow flux decay (α_2) likely caused by the continuous energy injection into the external shock. When this energy injection stops, a second break is then observed in the light curve ($t_{\rm break,2}$). This energy injection increases the energy of the afterglow shock by at least a factor of $f \gtrsim 4$, and augments the already severe requirements for the efficiency of the prompt gamma-ray emission.

Subject headings: gamma rays: bursts — radiation mechanisms: non thermal

1. Introduction

Gamma-ray bursts (GRBs) are believed to arise from the sudden release of a vast amount of energy ($\sim 10^{51}$ erg for long GRBs and probably somewhat less energy for short GRBs), into a very small region (of size $\lesssim 10^2$ km), over a short time ($\sim 10-10^2$ s for long GRBs and $\lesssim 1$ s for short GRBs). The prompt γ-ray emission is attributed to internal shocks within the outflow (Rees & Mészáros 1994; Sari & Piran 1997) that are caused by variability in its Lorentz factor, Γ. The highly non-thermal gamma-ray spectrum requires $\Gamma \gtrsim 10^2$ to avoid the *compactness problem* (see Piran 1999, and references therein). When the relativistic ejecta sweep a sufficient amount of external medium, they are decelerated by a (typically mildly relativistic) reverse shock; at the same time a highly relativistic forward shock is driven into the ambient medium. This forward shock produces the long-lasting afterglow emission, while the short lived reverse shock produces a prompt optical emission (*optical flash*); the latter peaks on a time scale of tens of seconds (Akerlof 1999; Sari & Piran 1999; Fenimore et al. 1999a; Soderberg & Ramirez-Ruiz 2002) and dominates the optical emission up to about ten minutes.

GRBs naturally divide into two classes according to their duration and the hardness of their prompt gamma-ray emission: short/hard bursts (< 2 s) and long/soft bursts (> 2 s) (Kouveliotou et al. 1993). Until very recently, afterglow emission was detected only for long GRBs, leading to significant progress in their understanding. To date over 50 spectroscopic

redshifts have been determined (typically $0.5 \lesssim z \lesssim 3$) and an association of some long GRBs with a contemporaneous Type Ic supernova (Stanek et al. 2003; Hjorth et al. 2003) has been established, which implies a massive star as the long GRB progenitor and thus, supports the collapsar model (Woosley 1993). The progenitors of short GRBs, on the other hand, remained until the launch of the *Swift* GRB observatory (Gehrels et al. 2004), largely a mystery. The leading short GRB model featuring the merger of a compact binary, usually NS-NS (e.g. Eichler et al. 1989) or NS-BH (e.g. Paczyński 1991), was given strong support recently with the detection of afterglow emission from three short GRBs: 050509B, 050709, and 050724 (Bloom et al. 2005; Gehrels et al. 2005; Hjorth et al. 2005; Lee et al. 2005; Berger et al. 2005; Barthelmy 2005).

Before *Swift*, X-ray afterglow emission was detected, in most cases, only several hours after the burst, by which time the flux typically showed a smooth single power law decay $\sim t^{-1}$. In contrast, the optical afterglow light curve often showed an achromatic steepening to $\sim t^{-2}$, attributed to a narrow jet whose edges become visible as it decelerates and widens (Rhoads 1999; Sari, Piran & Halpern 1999). However, the *early* afterglow evolution – the first few hours, which can probe important questions such as the density profile of the external medium and the early radiative energy losses from the external shock, remained largely unexplored. *Swift* is designed to, among other science, probe exactly this unknown observational time window from $\sim 10^2$ s to $\sim 10^4$ s after burst onset. Here we report for the first time cumulative early X-ray afterglow properties of the first 27 *long* GRBs detected with the *Swift*/XRT. In §2 we describe our data analysis method. Our observational results are presented in §3. In §4 we discuss the theoretical interpretation and implications of our findings, and our conclusions are summarized in §5.

2. Data Analysis

We have analyzed XRT data of the first 27 *Swift* GRB afterglows covering the time interval between December 2004 - June 2005. Data for each burst were obtained from the *Swift* Quick Look site[1] and processed consistently with version 2 of the *Swift* software (release date 2005-04-05). In all cases we used XSELECT to extract source and background counts from the cleaned event lists ($0.3 - 10$ keV), using grades 0-12 for Photon Counting (PC) mode data, 0-2 for Windowed Timing (WT) and 0-5 for Photo-Diode (PD). We used the European Southern Observatory (ESO) Munich Imaging Data Analysis System (MIDAS, version 04SEP), to create the X-ray afterglow light curves for each event. The data were

[1]http://heasarc.gsfc.nasa.gov/docs/swift/quicklook/

binned dynamically to have a certain number of photons per bin. For very bright bursts and at early times after a burst trigger, the binning was set to 500 photons per bin, while at very late times, or for very faint bursts the binning was set to 10 counts per bin. On the average, light curves were created with 50 counts per bin. All light curves were background subtracted. The exposure times per bin were calculated on the basis of the Good Time Interval (GTI) file. These light curves were then compared to ones derived independently with the FTOOL **flx2xsp**. Each time bin in the latter was selected for high signal to noise ratio, after background subtraction; we required at least 20 counts per bin in order to facilitate χ^2 fitting. The data sets derived using these two independent methods were found to agree very well. Finally, in both methods, we took into account the mode switching during the *Swift*/XRT observation, which can distort the real count rate during an event.

Several of the GRBs included in this paper were observed while *Swift* was still in its calibration phase, before the automatic mode-switching for the XRT was fully enabled. Some of the data obtained in PC mode suffered, therefore, from pile-up, which had to be corrected before the light-curves and spectra were fully analyzed. To account for source pileup (significant above 0.5 counts/s in Photon Counting mode), annular regions were used to extract the source spectra and light-curves. To determine the level of pile-up, the inner radius of the annulus was gradually increased until the spectral shape no longer changed (pile-up leads to the hardening of photon indices). Background spectra and light-curves were then produced from large 'source-free' regions, offset from the GRB, and the background counts were scaled to the same size region as used for the source.

The FTOOL **xrtmkarf** was used to generate ancillary response function (ARF) files. Where an annular region had been required, **xrtmkarf** was run twice, with and without the Point Spread Function (PSF) correction. Fitting the spectra with both ARFs leads to different normalizations, the ratio of which gives the pile-up correction factor. The most recent (version 7) response matrices (RMFs) were used in the spectral analysis. The light-curves were extracted for each individual orbit of data, correcting for pile-up when annuli were used. At later times, or when no pile-up was apparent, circles of radius 20-30 pixels (1 pixel = $2.36''$) were used.

The light-curves were converted into an XSPEC readable file and then modeled in XSPEC version 11.3.2 with a combination of single and broken power-laws to determine the decay slopes and break times. The time of the burst onset was taken from the msbal.fits TDRSS file, except for the case of GRB 050319, where the event started while *Swift* was slewing to a different target (although triggers are disabled during slews, the BAT triggered on a later peak in the light-curve of GRB 050319). To determine an energy conversion factor (ECF) from count-rate to fluxes, a simple absorbed (Galactic $N_{\rm H}$, determined from Dickey &

Lockman 1990, together with any required excess) power-law was fitted to the XRT spectra ($0.3 - 10$ keV). The ECFs were then determined for unabsorbed fluxes. If no significant spectral changes were observed, only one ECF was applied per light curve.

3. Observational Results

Until July 2005, only 10 *Swift* GRBs had measured redshifts. Figure 1 exhibits the evolution of the X-ray luminosities of these 10 *Swift* events together with the longest monitored GRBs in the last 8 years (see also Kouveliotou et al. 2004). The *Swift* light curves fill in the earlier gap and complete the trend observed in the past (Kouveliotou et al. 2004) in a spectacular way. Fig. 2 shows the evolution of the X-ray flux for the 17 *Swift* GRBs without known redshifts. Four of these events show X-ray flares early on (*lower panel* of Fig. 2).

Combining Figs. 1 and 2 we see that a general trend starts to emerge that may become the standard to describe each GRB X-ray afterglow light curve. Starting at the earliest XRT observations (approximately 10^2 s after the prompt gamma-rays), the X-ray flux F_ν follows a canonical behavior comprising three power law segments where $F_\nu \propto \nu^{-\beta} t^{-\alpha}$ (see also Fig. 3): an initial steep decay slope (α_1), which (at $t_{\rm break,1}$) changes into a very flat decay (α_2), that in turn (at $t_{\rm break,2}$) transitions to a slightly steeper slope (α_3). Table 1 lists the temporal and spectral parameters for all 27 events, as well as the break times ($t_{\rm break,1}$ and $t_{\rm break,2}$), the BAT trigger times, and the onset of the XRT data after trigger. The spectrum remained constant throughout the breaks (within our available statistics) in all cases except two (GRBs 050315 and 050319) where the spectrum hardened (i.e. β decreased) across the first break (at $t_{\rm break,1}$). Fig. 4 shows the distribution of all temporal indices (α_1, α_2 and α_3) together with the spectral index ($\beta_{\rm X}$) for the GRBs in Table 1.

Table 1 shows that in about half (40.7%) of the cases we were able to slew to the initial BAT location with XRT only several thousands of seconds after the GRB trigger; in the majority of these cases we detect one or even no temporal break in the X-ray afterglow light curve. In the latter cases (without a break) we have defined as α_3 the slope that prevails beyond 2×10^4 s in a light curve. It should be noted here that the values of α_3 are consistent with those seen in previous missions since they typically started observations hours after the burst.

Whenever we found early (< 500 s) breaks in the light curves of GRBs with established redshifts, we converted them in the GRB cosmological rest frame (below, but not in Table 1). We have three such cases, GRBs 050126, 050315, and 050319, with rest frame breaks at 185, 136, and 87 seconds, respectively. This sample, together with GRBs 050219A (≤ 332 s) and

050422 (≤ 272 s), strongly point to an early X-ray afterglow light curve break, $t_{\rm break,1} \lesssim 300$ s in the cosmological rest frame (or $t_{\rm break,1} \lesssim 500$ s in the observer frame). The distribution of $t_{\rm break,1}$ and $t_{\rm break,2}$ (without correcting for cosmological time dilation, since the redshift is not known for most of the GRBs in our sample) is shown in Figure 5.

We proceed to calculate the observed X-ray flux ($2-10$ keV) at 1 hr and 10 hr after the GRB trigger; whenever there was no direct measurement of the flux, we have used the temporal parameters of Table 1 to extrapolate to these times, using as a starting point the Spacecraft Clock trigger times (Table 1). We have used luminosity distances, d_L for $(\Omega_M, \Omega_\Lambda, h) = (0.3, 0.7, 0.71)$, and spectral parameters in order to calculate the isotropic equivalent X-ray luminosities at 1 hr ($L_{\rm X,1}$) and 10 hr ($L_{\rm X,10}$) and isotropic equivalent energy output in gamma-rays ($E_{\gamma,\rm iso}$). For the luminosities we used

$$L_{\rm X}(t) \equiv \int_{\nu_1}^{\nu_2} d\nu\, L_\nu(t) = \frac{4\pi d_L^2}{(1+z)} \int_{\nu_1}^{\nu_2} d\nu\, F_{\nu/(1+z)}[(1+z)t] = 4\pi d_L^2 \int_{\nu_1/(1+z)}^{\nu_2/(1+z)} d\nu\, F_\nu[(1+z)t]\ , \quad (1)$$

where $L_\nu(t)$ is the spectral luminosity at the cosmological rest frame of the source (i.e. both ν and t in $L_\nu(t)$ are measured in that frame), while $F_\nu(t)$ is measured in the observer's frame. When assuming $F_\nu \propto \nu^{-\beta} t^{-\alpha}$, Eq. 1 simplifies to $L_{\rm X}(t) = 4\pi d_L^2 (1+z)^{\beta-\alpha-1} F_{\rm X}(t)$, where $F_{\rm X}(t) = \int_{\nu_1}^{\nu_2} d\nu\, F_\nu(t)$.

The corresponding $L_{\rm x,1}$ and $L_{\rm x,10}$ ($2-10$ keV) were then calculated using the relevant spectral and temporal indices listed in Table 1. These values are listed in Table 2 together with the K-corrected values of $E_{\gamma,\rm iso}$ for each GRB. The latter has been recalculated within two energy bands, the narrowest of which ($100-500$ keV) overlaps in all GRBs. The wider band ($20-2000$ keV), is an upper limit and assumes no spectral changes from a single power law fit in the GRB prompt emission.

Figure 6 shows $L_{\rm X,10}$ versus $E_{\gamma,\rm iso}$ ($20-2000$ keV) for the 10 *Swift* GRBs with established redshifts, as well as 17 *HETE-II* and *BeppoSAX* GRBs ($20-2000$ keV), for comparison. The distribution of *Swift* events is compatible with that of earlier events measured with *HETE-II* and *BeppoSAX*; the combined sample is consistent with an apparent positive, roughly linear, correlation between $L_{\rm X,10}$ and $E_{\gamma,\rm iso}$. This suggests a high efficiency for the prompt gamma-ray emission, which is roughly constant (albeit with large scatter). Figure 6 also contains a color coding for the redshift of the different events; there is also an apparent positive correlation between $E_{\gamma,\rm iso}$ (or $L_{\rm X,10}$) and the redshift, z. This is likely due to observational selection effects, since, at least on average, intrinsically dimmer (brighter) events can be detected, their X-ray luminosity measured, and their redshift determined, out to a smaller (larger) redshift.

4. Theoretical Interpretation of the X-ray afterglow light curve

4.1. The Early Rapid Flux Decay (α_1)

The most natural explanation for the early rapid flux decay with $3 \lesssim \alpha_1 \lesssim 5$ is emission from *naked GRBs* (Kumar & Panaitescu 2000), i.e. prompt GRB emission (that is usually attributed to internal shocks) from large angles ($\theta > \Gamma^{-1}$) relative to our line of sight that reaches us at late times ($\Delta t \approx R\theta^2/2c$), resulting in a steep flux decay with $\alpha_1 = 2 + \beta_1$. This relation is more or less satisfied in most (though not all) cases for which α_1 could be determined (see Figure 7).

A somewhat steeper power law decay ($\alpha_1 > 2 + \beta_1$) can be obtained within a few $T_{\rm GRB}$, where $T_{\rm GRB}$ is the duration of the prompt emission, for the following reason. The temporal decay index of $\alpha_1 = 2 + \beta_1$ applies separately to each spike in the prompt light curve, as it corresponds to a collision between two sub-shells in the internal shocks models, where the emission from that collision decays as $F_\nu \propto (t - t_0)^{-\alpha_1}$. Here the reference time, t_0, of the power-law decay corresponds to the onset of that particular spike (i.e. the time at which the outer of the two sub-shells was ejected from the source). Since all power law fits to the light curve take the GRB trigger (which corresponds to the onset of the first spike) as the reference time, this would cause a seemingly steeper power law decay index for later spikes. The decay of the last spike, for which $t_0 \approx T_{\rm GRB}$, will approach a power-law decay in t for $t/T_{\rm GRB} \gtrsim$ a few. This would lead to a decrease in α_1 with time until it approaches $2 + \beta_1$ at $t/T_{\rm GRB} \gtrsim$ a few. Thus, if $t_{\rm break,1}/T_{\rm GRB} \lesssim$ a few, the asymptotic values of $\alpha_1 = 2 + \beta_1$ might not be reached. On the other hand, a shallower temporal decay index, $\alpha_1 < 2 + \beta_1$, is hard to achieve in this scenario, and might require a different physical origin. In practice, however, our mostly sparse coverage of the XRT light curves at $t < t_{\rm break,1}$ might lead to an underestimation of α_1, since the value that is derived from the fit to the data may not represent its asymptotic value at $t \ll t_{\rm break,1}$.

Assuming that the *naked GRB* interpretation is correct, we expect $F_\nu(t < t_{\rm break,1})$, or its extrapolation back in time, to smoothly join with the prompt GRB emission as the emission immediately after the burst would be dominated by the tail of the last spike. At later times, $t \gtrsim 2T_{\rm GRB}$, the light curve would have contributions from the tails of all spikes with a relative weight similar to that of the spikes themselves. This indeed seems to be the case in most *Swift* GRBs for which an XRT light curve at $t < t_{\rm break,1}$ is available (e.g., Vaughan et al. 2005; Tagliaferri et al. 2005).

An interesting alternative model for the initial fast decay, that might apply at least in some cases, is reverse shock emission from large angles relative to our line of sight (Kobayashi et al. 2005). This emission might be either synchrotron or synchrotron self-Compton (SSC).

The latter could suppress the flux in the optical relative to that in the X-rays (Kobayashi et al. 2005), thus supporting the strict upper limits on the early optical flux that exist for some of the GRBs in our sample. This interpretation would require, however, a large Compton y-parameter, and in turn a very low magnetization of the GRB outflow. The synchrotron component of the reverse shock emission could dominate in the X-ray range. This is theoretically possible despite the fact that the F_ν spectrum peaks around the optical or IR, since the νF_ν spectrum peaks closer to the X-ray range and is fairly flat above its peak, so that a good fraction of the total emitted energy can fall within the X-ray range.

Finally, several other models can also be considered to explain this part of the X-ray light curve (Tagliaferri et al. 2005). For example, emission from the hot cocoon in the context of the collapsar model (Mészáros & Rees 2001; Ramirez-Ruiz, Celloti & Rees 2002) might produce a sufficiently steep flux decay, but would naturally produce a quasi-thermal spectrum which does not agree with the observed power-law spectrum. Photospheric emission as the ejecta becomes optically thin (Rees & Mészáros 2005; Ramirez-Ruiz 2005) is also possible as it may be able to produce significant deviations from a thermal spectrum although it is unclear how this emission would last longer than the prompt gamma-ray emission itself. Tagliaferri et al. (2005) have also suggested that the *patchy shell* model (Kumar & Piran 2000b), where there are angular inhomogeneities in the outflow, might produce a sufficiently fast decay if our line of sight is within a *hot spot* in the jet, of angular size $\sim \Gamma^{-1}$, causing a mini-jet break as the flow is decelerated by the external medium. However, this would produce $\alpha_1 \lesssim p \sim 2-2.5$ (where p is the power law index of the electron energy distribution), which is significantly lower than the typical observed values of $3 \lesssim \alpha_1 \lesssim 5$. Furthermore, this would require an extreme angular inhomogeneity in the outflow. The *patchy shell* model, however, would naturally produce a series of bumps and wiggles in the light curve on top of a more moderate underlying power law flux decay (Fenimore et al. 1999b; Nakar, Piran & Granot 2003) (rather than the observed smooth and very steep decay which later turns into a smooth and very shallow decay). From all the above, we conclude that while different mechanisms might still be responsible for the steep early flux decays in the X-ray afterglows of some GRBs, emission for *naked GRBs* is the most promising mechanism, and is likely at work in most cases.

4.2. The First Break in the Light Curve ($t_{\rm break,1}$)

Between $t_{\rm break,1} < t < t_{\rm break,2}$ there is a very shallow decay of the flux, with $0.2 \lesssim \alpha_2 \lesssim 0.8$. We interpret the first break, at $t_{\rm break,1}$, as the time when the slowly decaying emission from the forward shock becomes dominant over the rapidly decaying flux from the prompt

emission at large angles from our line of sight. This break can generally be chromatic, if the spectrum of the prompt emission at large angles (which corresponds to a larger frequency range in the local frame compared to the observed frequency during the prompt emission) has a different spectral slope in the X-rays than the afterglow emission from the forward shock. Under this interpretation, we do not expect a break in the optical (or UV, or IR) light curve at exactly the same time as in the X-rays (except for the rare cases where by coincidence the spectra of these two distinct physical regions are similar over such a large range in frequencies). This prediction could serve as a diagnostic test for our interpretation.

Out of six GRBs for which $t_{\rm break,1}$ was well determined, two events (050315 and 050319) show clear evidence for a change of the spectral slope in the X-ray range, $\beta_{\rm X}$, across the break (with $\Delta\beta_{\rm x} \equiv \beta_{\rm X,2} - \beta_{\rm X,1}$ of -0.5 and -0.9, respectively).[2] In the other four cases, while there is no evidence for a change in $\beta_{\rm X}$ across the break, such a change can only be constrained to $|\Delta\beta_{\rm X}| \lesssim 0.3$. Thus we consider the observed behavior of $\beta_{\rm X}$ across $t_{\rm break,1}$ to be broadly consistent with our interpretation, in which $|\Delta\beta_{\rm X}|$ is not expected to always be very large, and can in many cases be rather modest.

The fact that the sharply decaying flux from the prompt emission initially (at $t < t_{\rm break,1}$) dominates over the emission from the external shock, suggests that either (i) the prompt emission dissipates and radiates most of the initial energy in the outflow, leaving a much smaller energy in the external shock, or (ii) the energy that is dissipated in the prompt emission (i.e. the kinetic energy that is converted to internal energy) is comparable to that in the forward shock, but the fraction of that energy which is radiated in the observed band is much larger for the prompt emission. The latter is relevant for the internal shocks model, in which at most about half (and typically much less) of the initial kinetic energy is expected to be converted to internal energy in the internal shocks, while most of the remaining energy (which is expected to be close to the original energy) is converted to internal energy in the external shock. The emission from the forward shock peaks at the deceleration time (when the ejecta slow down significantly and most of their energy is transfered to the forward shock), $t_{\rm dec}$, which is comparable to the duration of the GRB, $T_{\rm GRB}$, for a mildly relativistic reverse shock, so that a comparable radiative efficiency would lead to a comparable bolometric luminosity (assuming a similar fraction of the internal energy goes to electrons and is radiated away). Thus, the larger flux from the internal shocks suggests that a higher fraction of the internal energy is converted into radiation in the observed band. The high efficiency that is required from the prompt gamma-ray emission is further discussed in §4.3.

[2]These two GRBs also have a rather steep early decay with $\alpha_1 \approx 4$, which supports the interpretation of *naked GRB* emission.

4.3. Intermediate Shallow Flux Decay (α_2)

In most cases α_2 is too small ($0.2 \lesssim \alpha_2 \lesssim 0.8$) to reasonably account for with an adiabatic evolution of the forward shock with a constant energy (Sari, Piran & Narayan 1998; Granot & Sari 2002, see also §4.4), while radiative losses would only cause a steeper flux decay. This suggests instead a gradual energy injection during this part of the X-ray light curve, which can take place in two main forms: (i) toward the end of the burst the Lorentz factor Γ of the outflow that is being ejected decreases with time, forming a smooth distribution of ejected mass as a function of its Lorentz factor, $M(>\Gamma)$, and its corresponding energy, $E(>\Gamma)$. In this picture Γ increases with radius R and material with Lorentz factor Γ catches up with the forward shock when the Lorentz factor of the forward shock, Γ_f, drops slightly below Γ (Rees & Mészáros 1998; Sari & Mészáros 2000; Ramirez-Ruiz, Merloni & Rees 2001), resulting in a smooth and gradual energy injection into the afterglow shock. (ii) An alternative scenario for the energy injection is that the central source remains active for a long time (Rees & Mészáros 2000; MacFadyen et al. 2001; Ramirez-Ruiz 2004; Lee & Ramirez-Ruiz 2002). Here the ejected outflow has a Lorentz factor, Γ_i, that is much larger than that of the forward shock when it catches-up with it, $\Gamma_i \gg \Gamma_f$. This leads to a more highly relativistic reverse shock (with a Lorentz factor $\Gamma_r \sim \Gamma_i/2\Gamma_f \gg 1$) compared to scenario (i) where the reverse shock is only mildly relativistic, thus resulting in a significantly different emission from the reverse shock (which becomes similar to that from the forward shock for $\Gamma_r \sim \Gamma_f$, assuming a similar composition and similar micro-physical parameters in both shocks).

Scenario (ii) requires the central engine to remain active for a very long time, up to $t_{\rm break,2}$, which is in many cases several hours (see Table 1 and Figure 5). Interestingly enough, the X-ray flares in the early afterglow light curve of some GRBs also suggest that the central source remains active for hours after the GRB (see §4.5). The main difference is that scenario (ii) requires both smooth and continuous (rather than episodic) energy injection by the source at late times, and that it also requires most of the energy to be injected at late times, hours after the GRB.

Below, we assume for simplicity that the emission in the X-ray range is dominated by the forward shock, rather than by the reverse shock, which is typically expected to be the case.

In scenario (i), the power law flux decay of the X-ray afterglow suggests power law dependences of $M(>\Gamma) \propto \Gamma^{-s}$ and $E(>\Gamma) \propto \Gamma^{1-s}$. In order to affect the forward shock dynamics, slow down its deceleration, and cause a shallower flux decay, the total energy

in the afterglow shock should gradually increase with time.[3] This implies that the total injected energy, $E_i(t)$, must first exceed the initial energy, E_0, in the afterglow shock before it significantly effects its dynamics. Therefore, the flattening of the light curve would start at t_i for which $E_i(t_i) \sim E_0$. Neglecting radiative losses we have $E(t) = E_0 + E_i(t)$, so that $E(t) \approx E_i(t)$ for $t > t_i$. Furthermore, $E_i(t)$ should gradually increase with time, implying $s > 1$. For simplicity spherical symmetry is assumed below, but the results are also valid for a uniform jet (viewed from within its aperture) as long as the Lorentz factor exceeds the inverse of the jet half-opening angle, and when the energy is replaced by the isotropic equivalent energy. For any given power law segment of the spectrum we have $F_\nu \propto E^b t^{-\alpha_{\rm ad}}$ where $\alpha_{\rm ad}$ is the temporal decay index for an adiabatic shock evolution (with no energy injection or radiative losses) which is given in Eq. 7, while $E(t > t_i) \propto t^a$ with $a = (s-1)(3-k)/(7+s-2k)$ for energy injection with an external density profile $\rho_{\rm ext} = Ar^{-k}$ (Sari & Mészáros 2000). For the relevant power law segments of the spectrum,

$$b = \begin{cases} 3/4 = 3\beta/2 & \nu_c < \nu < \nu_m \quad (k < 3)\ , \\ (3+p)/4 = (\beta+2)/2 & \nu_m < \nu < \nu_c \quad (k = 0)\ , \\ (1+p)/4 = (\beta+1)/2 & \nu_m < \nu < \nu_c \quad (k = 2)\ , \\ (2+p)/4 = (\beta+1)/2 & \nu > \max(\nu_m, \nu_c) \quad (k < 3)\ , \end{cases} \tag{2}$$

(Granot & Sari 2002). The increase in the temporal decay index across the break at $t_{\rm break,2}$ is $\Delta\alpha \equiv \alpha_3 - \alpha_2 = a\,b$. Thus, we can obtain the power law index of the energy injection, s, as a function of β [or $b(\beta)$] and $\Delta\alpha$ which may be directly measured from observations,

$$s = 1 + \frac{2(4-k)\Delta\alpha}{(3-k)b(\beta) - \Delta\alpha}\ . \tag{3}$$

One can determine the power law segment in which the X-ray band is located, and thus the appropriate expression for $b(\beta)$ (see Eq. 2), from the relations between α_3 and β_3 (see §4.4). Figure 8 shows the values of (α_3, β_3) for the events for which $t_{\rm break,2}$ could be determined, along with the expected relations for the potentially relevant power law segments of the spectrum. There are nine such events, and they all fall reasonably close to these relations.

[3]This is valid also when there are radiative losses, in which case an increase with time in the energy of the afterglow shock would require a faster energy injection rate, corresponding to a higher minimal value of s, compared to the requirement $s > 1$ for the adiabatic case. For simplicity we neglect radiative losses in the following analysis.

Table 3 gives the derived values of s. In this scenario it should be noticed that $s > 1$ so that the value of a is bound within the range $0 < a < (3-k)$, and correspondingly

$$0 < \Delta\alpha < \Delta\alpha_{\rm max} = (3-k)b(\beta) \ , \tag{4}$$

where $\Delta\alpha$ approaches $\Delta\alpha_{\rm max}$ for $s \gg 1$. The limits on the possible values of $\Delta\alpha$ in scenario (i) are more constraining for a stellar wind environment ($k = 2$) for which $0 < \Delta\alpha < b(\beta) \sim 1$, compared to a uniform external density ($k = 0$). We find only the high redshift GRB 050505 not to be compatible with this constraint.[4]

On the other hand, in order to reproduce the observed power law decay of the X-ray flux in scenario (ii), the (kinetic) luminosity of the central source should be a power law in the lab frame time $t_{\rm lab}$ (for which $R \approx ct_{\rm lab}$), $L \propto t_{\rm lab}^{q}$. In this case $\Gamma \propto R^{-(2-q-k)/2(2+q)} \propto t^{-(2-q-k)/2(4-k)}$ (Blandford & McKee 1976) and $E \propto t^{q+1}$, i.e. $a = q + 1$. Therefore, for scenario (ii) we have the relatively simple relation,

$$q = \frac{\Delta\alpha}{b(\beta)} - 1 \ . \tag{5}$$

Table 3 gives the required values of q for various bursts in our sample. It is interesting to note that in scenario (ii) there is no upper bound on the value of a or on the values of $\Delta\alpha = a\, b(\beta)$, but only a trivial lower limit ($a > 0$ and $\Delta\alpha > 0$). This is in contrast with scenario (i) where $\Delta\alpha$ has an upper limit of $\Delta\alpha_{\rm max} = (3-k)b(\beta)$ (see Eq. 4). Therefore, if $\Delta\alpha$ exceeds $\Delta\alpha_{\rm max}$ for some GRB, this could be explained only by scenario (ii), and not by scenario (i). This can potentially serve as a diagnostic method for distinguishing between these two types of energy injection into the forward shock.

In both scenarios discussed above, the total amount of injected energy must increase with time (and exceed the initial energy in the afterglow shock) to effect the dynamics of the afterglow shock and cause a shallower flux decay. In scenario (ii), this implies $q > -1$, which is not a trivial requirement, and is hard to produce in many GRB progenitor models. For example, in the collapsar model the late time accretion rate due to fallback is expected to scale with time as $\dot{M}_{\rm acc} \propto t_{\rm lab}^{-5/3}$ (MacFadyen et al. 2001), which for a roughly constant efficiency, η, implies $L = \eta \dot{M}_{\rm acc} c^2 \propto t_{\rm lab}^{-5/3}$ and $q = -5/3$. For the magnetar model (Zhang & Mészáros 2001; Rosswog et al. 2003; Usov 1992; Dai & Lu 1998), L is initially constant while after the newly born neutron star spins down significantly, $L \propto t_{\rm lab}^{-2}$, i.e. $q = -2$. Thus, both these models could not naturally explain the flatter flux decays at $t_{\rm break,1} < t < t_{\rm break,2}$ due to late time energy injection from the source (see Table 3).

[4]The reader should, however, keep in mind that for this event the determination of $t_{\rm break,2}$ is uncertain given the intrinsic curvature of the afterglow lightcurve.

Regardless of the exact details of the energy injection, we can constrain the factor f by which the energy of the afterglow shock was increased due to the energy injection [$f = (E_0 + E_{\rm injected} - E_{\rm radiated})/E_0$ where $E_{\rm injected} = E_i(t_f)$]. If the energy injection lasted between t_i and t_f, it would cause a flux increase by a factor of $(t_f/t_i)^{\Delta\alpha}$ compared to the hypothetical case of no energy injection (or radiative losses), corresponding to $f = (t_f/t_i)^{\Delta\alpha/b(\beta)}$. While t_f is identified with $t_{\rm break,2}$, we do not know the exact value of t_i. We do, however, know that $t_i < t_{\rm break,1}$, and $t_i \gtrsim T_{\rm GRB}$, which provide the following constraints on f,

$$\left(\frac{t_{\rm break,2}}{t_{\rm break,1}}\right)^{\Delta\alpha/b(\beta)} < f \lesssim \left(\frac{t_{\rm break,2}}{T_{\rm GRB}}\right)^{\Delta\alpha/b(\beta)} \quad . \tag{6}$$

The energy in the afterglow at late times (later than several hours and therefore at $t > t_{\rm break,2}$) is typically estimated to be comparable to or smaller than that in the prompt gamma-ray emission (Panaitescu & Kumar 2002; Lloyd-Ronning & Zhang 2004), even when correcting for radiative losses from the afterglow shock at early times, implying a high efficiency for the prompt emission, which is $\gtrsim 50\%$ in most cases. This is in particular a serious problem for the internal shocks model, where it is hard to reach such high efficiencies in converting the bulk kinetic energy of the outflow to the observed gamma-rays (Kumar 1999; Gueta, Spada & Waxman 2001). The energy injection interpretation implies that most of the energy in the afterglow shock at late times was either (i) originally in material with an initial Lorentz factor $\Gamma < 10^2$ which could therefore have not contributed to the prompt gamma-ray emission (due to the compactness problem; see Lithwick & Sari 2001, and references therein), or (ii) injected at late times, after the prompt gamma-ray emission was over.

This requires the prompt gamma-ray emission to be significantly more efficient than previous estimates, where E_γ/E_0 increases by a factor of $f \gtrsim 4$ (see Table 3). Furthermore, we find that the energy of the afterglow shock increases by a factor of f when also taking into account radiative losses, while most previous estimates of E_γ/E_0 included the radiative losses assuming that they decrease the energy of the afterglow shock by a factor of ~ 3 or so. Therefore, the correction for E_γ/E_0 compared to such previous estimates would be even larger (by a factor of $\sim 3f$). The efficiency of the prompt gamma-ray emission is usually defined as $\epsilon_\gamma \equiv E_\gamma/(E_\gamma + E_0) = 1/(1 + E_0/E_\gamma)$. Thus, previous estimates which typically gave $E_\gamma/E_0 \gtrsim 1$ and $\epsilon_\gamma \gtrsim 50\%$ would now, with a correction factor of $\sim 3f \gtrsim 10$, imply $\epsilon_\gamma \gtrsim 90\%$. This poses severe requirements for theoretical models.

4.4. Second Break in the Light Curve ($t_{\rm break,2}$) into a Steeper Flux Decay (α_3)

When energy injection ends, at $t > t_{\rm break,2}$, an adiabatic evolution of the forward shock at a constant energy follows, producing a somewhat steeper decay slope, α_3 (Sari, Piran & Narayan 1998; Granot & Sari 2002). The relations between the temporal and spectral indices for the power law segments of the spectrum that might be relevant in the X-rays are

$$\alpha = \begin{cases} 1/4 & = & \beta/2 & \nu_c < \nu < \nu_m & (k<3)\ , \\ 3(p-1)/4 & = & 3\beta/2 & \nu_m < \nu < \nu_c & (k=0)\ , \\ (3p-1)/4 & = & (3\beta+1)/2 & \nu_m < \nu < \nu_c & (k=2)\ , \\ (3p-2)/4 & = & (3\beta-1)/2 & \nu > \max(\nu_m,\nu_c) & (k<3)\ . \end{cases} \tag{7}$$

In this picture $t_{\rm break,2}$ corresponds, for the two scenarios described in §4.3, respectively, to (i) the time when the energy injection to the forward shock ends, i.e. when the Lorenz factor of the forward shock drops to slightly below the minimal Lorentz factor, $\Gamma_{\rm min}$, of the ejecta which carry significant energy, and (ii) the time when the central source becomes inactive. Under both of the energy injection scenarios, the second break (at $t_{\rm break,2}$) should be achromatic, as long as the emission before the break was dominated by the forward shock rather than by the reverse shock. If the emission before the break is dominated by the reverse shock, then there should be a brief period of fast decay of the flux (from the reverse shock), as the supply of newly shocked outflow ends, and the existing shocked outflow cools adiabatically (and radiatively). This short phase ends once the emission becomes dominated by the forward shock. During this short intermediate period the light curve could show chromatic behavior.

Assigning a Lorentz factor to a given observed time is not uniquely defined, since photons from a wide range of radii and Lorentz factors reach the observer simultaneously. One can parameterize $t/(1+z) = R/C\gamma^2 c$, where the uncertainty is put into the value of the parameter C. Using the Blandford & McKee (1976) self-similar solution as a guide, and evaluating the Lorentz factor just behind the shock, this gives

$$\gamma = \left[\frac{(17-4k)E(1+z)^{3-k}}{16C^{3-k}\pi c^{5-k}t^{3-k}}\right]^{1/2(4-k)}\ . \tag{8}$$

Estimating the typical Lorentz factor for a given observed time as that just behind the shock at the radius corresponding to the outer edge of the afterglow image (Granot & Sari 2002)

gives $C = 4(4-k)/(5-4)$ and in turn,

$$\gamma(t) = \begin{cases} 6.68(E_{52}/n_0)^{1/8}[t_{\rm days}/(1+z)]^{-3/8} & (k=0)\ , \\ \\ 4.90(E_{52}/A_*)^{1/4}[t_{\rm days}/(1+z)]^{-1/4} & (k=2)\ , \end{cases} \tag{9}$$

while simply parameterizing $C = 4C_4$ gives

$$\gamma(t) = \begin{cases} 6.14\, C_4^{-3/8}(E_{52}/n_0)^{1/8}[t_{\rm days}/(1+z)]^{-3/8} & (k=0)\ , \\ \\ 4.43\, C_4^{-1/4}(E_{52}/A_*)^{1/4}[t_{\rm days}/(1+z)]^{-1/4} & (k=2)\ , \end{cases} \tag{10}$$

where $t_{\rm days} = t/(1\ {\rm day})$, $n = n_0\ {\rm cm}^{-3}$ is the external number density for $k = 0$, $A_* = A/(5\times 10^{11}\ {\rm g\ cm}^{-1})$ for $k = 2$, and $E_{52} = E/(10^{52}\ {\rm erg})$. In scenario (i) one may estimate $\Gamma_{\rm min} \approx 2\gamma(t_{\rm break,2})$, using equations 9 or 10 for $\gamma(t)$. Typical values are $15 \lesssim \Gamma_{\rm min} \lesssim 50$ for $k = 0$ and $10 \lesssim \Gamma_{\rm min} \lesssim 20$ for $k = 2$ [for $E_{52}/n_0 \sim 1$, $E_{52}/A_* \sim 1$ and $0.2 \lesssim t_{\rm break,2}/(10^4\ {\rm s}) \lesssim 4$].

Optical afterglows typically show a jet break at $t_{\rm jet}$ which can range from several hours to weeks, and typically occurs after $t_{\rm break,2}$. Thus, it might be possible in some cases to see the jet break at $t_{\rm jet} > t_{\rm break,2}$, as might be the case for GRB 050315 Vaughan et al. (2005).

4.5. X-ray Flares in the Early Afterglow

The early X-ray light curves obtained with *Swift* XRT often show flares (see *lower panel* of Fig. 2). The most prominent flare so far was in GRB 050502B, where the flux increased by a factor of ~ 500. Some of these flares have very sharp temporal features where the flux changes significantly on time scales $\Delta t \ll t$ (Burrows et al. 2005). Most flares have a very steep rise and decay (with very large temporal rise/decay indices when fitted to a power law). When the flare is bright enough to follow its spectral evolution, its hardness ratio evolves during the flare, and its spectral index is somewhat different than the one associated with the underlying power law decay of the X-ray light curve before and after the flare (Burrows et al. 2005). Furthermore, the fluxes before and after the flare lie approximately on the same power law decay, suggesting that the flare originates from a distinct physical component than that responsible for the underlying power law decay.

It is very difficult (nearly impossible under realistic conditions) to produce very sharp temporal variations of the flux ($\Delta t \ll t$) with large amplitudes ($\Delta F \gtrsim F$) in the external shock, be it from refreshed shocks [5] (Kumar & Piran 2000a; Granot, Nakar & Piran 2003;

[5]Refreshed shocks that occur after the jet break in the light curve, could produce $\Delta F \gtrsim F$ on time scales

Ramirez-Ruiz, Merloni & Rees 2001), bumps in the external medium (Lazzati et al. 2002; Nakar, Piran & Granot 2003; Ramirez-Ruiz et al. 2001) or angular inhomogeneities in the outflow (Fenimore et al. 1999b; Nakar, Piran & Granot 2003). Therefore, the most likely explanation for these flares is late internal shocks. This implies that the central source is still active at relatively late times.

5. Conclusions

We have presented X-ray light curves for 27 GRBs monitored by *Swift* XRT during December 2004 - June 2005. These light curves start as early as $\lesssim 10^2$ s after the GRB trigger, and cover up to four decades in time. The most striking result we obtain is that the early X-ray light curves show a canonical behavior (see Figs. 1, 2 and 3) which consists of three power law segments: an initial very steep decay ($F_\nu \propto \nu^{-\beta} t^{-\alpha}$ with $3 \lesssim \alpha_1 \lesssim 5$), followed by a very shallow decay ($0.2 \lesssim \alpha_2 \lesssim 0.8$), and finally a somewhat steeper decay ($1 \lesssim \alpha_3 \lesssim 1.5$). These three power law segments of the early X-ray light curve meet at two break times, 300 s $\lesssim t_{\rm break,1} \lesssim$ 500 s, and 10^3 s $\lesssim t_{\rm break,2} \lesssim 10^4$ s. All the light curves in our sample are consistent with this basic picture of a canonical light curve, although in many cases we do not see all three power law segments, due to limited temporal coverage.

The large variety of behaviors exhibited by afterglows, while clearly compatible with relativistic fireball models, poses new challenges of interpretation. We find that the most promising explanation for the initial fast flux decay (α_1) is that it is the tail of the prompt gamma-ray emission which is emitted from large angles ($\theta > \Gamma^{-1}$) relative to our line of sight (Kumar & Panaitescu 2000). This model produces a sharp flux decay with $\alpha_1 = 2 + \beta_1$, in rough agreement with observations (Fig. 7), while $\alpha_1 > 2 + \beta_1$ might also be expected for $t/T_{\rm GRB} \lesssim$ a few (see §4.1).

The shallow intermediate flux decay (α_2) is most likely caused by continuous energy injection into the forward shock. This energy injection is probably due to a decrease in the Lorentz factor, Γ, of the outflow toward the end of the prompt GRB, resulting in a monotonic increase of Γ with radius. This outflow gradually catches up with the afterglow shock, resulting in a smooth energy injection (Sari & Mészáros 2000). This picture requires $E(>\Gamma) \propto \Gamma^{1-s}$ with $s > 1$. We have deduced the values of s from the observed X-ray light curves (see Table 3) and typically obtain $s \sim 2.5$.

$\Delta t/t$ as small as $\sim 0.15 - 0.2$ with (Granot, Nakar & Piran 2003), corresponding to the ratio of the radial and angular times. The X-ray flares, however, typically occur at early times, before the jet break time, so that we expect $\Delta t/t \sim 1$ for refreshed shocks.

Energy injection could also be caused by a long lasting activity of the central source, which keeps ejecting significant amounts of energy in a highly relativistic outflow up to several hours after the GRB. However, this requires the source luminosity to decay very slowly with time, $L \propto t_{\rm lab}^{q}$ with $q > -1$, where most of the energy is extracted near $t_{\rm break,2}$, i.e. up to several hours after the GRB. Therefore, we find this option not very promising. One might be able to distinguish between these two scenarios for energy injection by the help of early broad band observations, since the emission from the reverse shock is expected to be different for these two cases. Furthermore, the change in the temporal index, $\Delta\alpha$, across the second break in the light curve at $t_{\rm break,2}$ is bounded in the first scenario (see Eq. 4) but not in the second scenario. In all the GRBs in our sample for which it could be tested (perhaps with one exception, GRB 050505), the value of $\Delta\alpha$ falls within the allowed range for the first scenario.

The third power law segment of the light curve (α_3) is most likely the well known afterglow emission from a spherical adiabatic external shock (Sari, Piran & Narayan 1998; Granot & Sari 2002). The observed values of the temporal index (α_3) and the spectral index (β_3) are consistent with this interpretation (see Fig. 8).

In some cases flares are seen on top of the basic canonical light curve that is illustrated in Fig. 3, as can be seen in the *lower panel* of Fig. 2. These flares are most likely caused by internal shocks within the outflow that is ejected from the central source at late times (very close to the time when these flares are seen). This implies the the central source quite often remains active for hours after the GRB.

We find evidence for a change in the spectral slope across the first break in the light curve ($t_{\rm break,1}$) in two out of six cases for which we could determine $t_{\rm break,1}$. This is consistent with our interpretation in which the first break occurs when the slowly decaying emission from the forward shock becomes dominant over the steeply decaying tail emission of the prompt GRB from large angles with respect to our line of sight. Since these two components arise from physically distinct regions, their spectrum would generally be different. We find no evidence for a change in the spectral slope across the second break in the light curve ($t_{\rm break,2}$). This is consistent with our interpretation where this break is caused by the end of the energy injection into the forward shock, as long as the emission before the break (at $t_{\rm break,1} < t < t_{\rm break,2}$) is dominated by the forward shock (rather than by the reverse shock), which is typically expected to be the case in the X-ray band.

Finally, the interpretation of the shallow intermediate flux decay as caused by energy injection, implies that the energy in the afterglow shock at late times (more than several hours) is larger than that at the deceleration time by a factor of $f \gtrsim 4$ (see Eq. 6 and Table 3). As discussed at the end of §4.3, this requires the prompt gamma-ray emission to be

extremely efficient, and typically convert $\gtrsim 90\%$ of the total energy in the highly relativistic outflow (with $\Gamma \gtrsim 10^2$) that is ejected during the GRB itself into the observed gamma-rays. If a significant fraction of the radiated energy goes to photon energies above the observed range, the efficiency requirements of the prompt emission become even more severe.

The authors acknowledge support from ASI, NASA and PPARC, and benefits from collaboration within the EC FP5 Research Training Network "Gamma-Ray Bursts – An Enigma and a Tool". C. K., S. K. P. and J. G. acknowledge the hospitality of the Institute of Advanced Study in Princeton, during the preparation of this paper. This research was supported by US Department of Energy under contract number DE-AC03-76SF00515 (J.G.), by NASA through a Chandra Postdoctoral Fellowship award PF3-40028 (E. R.-R.), and by NASA grant NAS5-00136 (D. G., D. B., J. N.).

REFERENCES

Akerlof, C., et al. 1999, Nature, 398, 400

Barthelmy, S. et al. 2005, submitted to Nature

Berger, E., Kulkarni, S. R., & Frail, D. A. 2003, ApJ, 590, 379

Berger, E., et al. 2005, submitted to Nature (astro-ph/0508115)

Blandford, R. D., & McKee, C. F. 1976, Phys. of Fluids, 19, 1130

Bloom, J. S., Frail, D. A., & Kulkarni, S. R. 2003, ApJ, 594, 674

Bloom, J. S., et al. 2005, submitted to ApJ (astro-ph/0505480)

Burrows, D. N., et al., 2005, submitted (astro-ph/0506130)

Dai, Z. G., & Lu, T., 1998, Phys. Rev. Lett., 81, 4301

Dickey & Lockman 1990, ARA & A, 28, 215

Eichler, D., Livio, M., Piran, T., & Schramm, D. N. 1989, Nature, 340, 126

Fenimore, E. E., Ramirez-Ruiz, E., & Wu, Bobing 1999, 518, L73

Fenimore, E. E., Cooper, C., Ramirez-Ruiz, E., Sumner, M. C., Yoshida, A., & Namiki, M. 1999, 512, 683

Galama, T. J., & Wijers, R. A. M. J. 2001, ApJ, 549, L209

Gehrels, N., et al. 2004, ApJ, 611, 1005

Gehrels, N., et al. 2005, submitted (astro-ph/0505630)

Granot, J., & Sari, R. 2002, ApJ, 568, 820

Granot, J., Nakar, E., & Piran, T. 2003, Nature, 426, 138

Guetta, D., Spada, M., & Waxman, E. 2001, ApJ, 557, 399

Hjorth, J., et al. 2003, Nature, 423, 847

Hjorth, J., et al. 2005, ApJL, in press (astro-ph/0506123)

Kobayashi, S., Zhang, B., Mészáros, P., & Burrows, D. N. 2005, submitted to ApJL (astro-ph/0506157)

Kouveliotou, C., et al. 1993, ApJ, 413, L101

Kouveliotou, C., et al. 2004, ApJ, 608, 872

Kumar, P. 1999, ApJ, 523, L113

Kumar, P., & Panaitescu, A. 2000, ApJ, 541, L51

Kumar, P., & Piran, T. 2000a, ApJ, 532, 286

Kumar, P., & Piran, T. 2000b, ApJ, 535, 152

Lazzati, D., et al. 2002, A&A, 396, L5

Lee, W. H., & Ramirez–Ruiz, E. 2002, ApJ, 575, 893

Lee, W. H., Ramirez-Ruiz, E., & Granot, J. 2005, ApJ in press (astro-ph/0506104)

Lithwick, Y., & Sari, R. 2001, ApJ, 555, 540

Lloyd-Ronning, N. M., & Zhang, B. 2004, ApJ, 613, 477

MacFadyen, A. I., Woosley, S. E., & Heger, A. 2001, ApJ, 550, 410

Mészáros, P., & Rees, m. J. 2001, ApJ, 556, L37

Nakar, E., Piran, T., & Granot, J. 2003, New Astron., 8, 495

Paczyński, B. 1991, Acta Astron., 41, 257

Panaitescu, a., & Kumar, P. 2002, ApJ, 571, 779

Piran, T. 1999, Physics Reports, 314, 575

Ramirez-Ruiz, E., Merloni, A., & Rees, M. J. 2001, MNRAS, 324, 1147

Ramirez-Ruiz, E., Dray, L., Madau, P., & Tout, C., 2001, MNRAS, 327, 829

Ramirez-Ruiz, E., Celotti, A., & Rees, M. J. 2002, MNRAS, 337, 1349

Ramirez-Ruiz, E. 2004, MNRAS, 349, L38

Ramirez-Ruiz, E. 2005, MNRAS in press

Rees, M. J., & Mészáros, P. 1994, ApJ, 430, L93

Rees, M. J., & Mészáros, P. 1998, ApJ, 496, L1

Rees, M. J., & Mészáros, P. 2000, ApJ, 545, L73

Rees, M. J., & Mészáros, P. 2005, ApJ, 628, 847

Rhoads, J. E. 1999, ApJ, 525, 737

Rosswog, S., Ramirez-Ruiz, E., & Davies, M. B. 2003, MNRAS, 345, 1077

Sari, R., & Mészáros, P. 2000, ApJ, 535, L33

Sari, R., & Piran, T. 1997, ApJ, 485, 270

Sari, R., & Piran, T. 1999, ApJ, 517, L109

Sari, R., Piran, T., & Halpern, J. P. 1999, ApJ, 519, L17

Sari, R., Piran, T., & Narayan, R. 1998, ApJ, 497, L17

Soderberg, A. M., & Ramirez-Ruiz, E. 2002, MNRAS, 330, L24

Stanek, K., et al. 2003, ApJ, 591, L17

Tagliaferri, G., et al. 2005, Nature in press (astro-ph/0506355)

Thompson, T. A., Chang, P., & Quataert, E. 2004, ApJ, 611, 380

Usov, V. V. 1992, Nature, 357, 472

Vaughan, S., et al. 2005, submitted

Woosley, S. E. 1993, ApJ, 405, 273

Zhang, B., Mészáros, P. 2001, ApJ, 552, L35

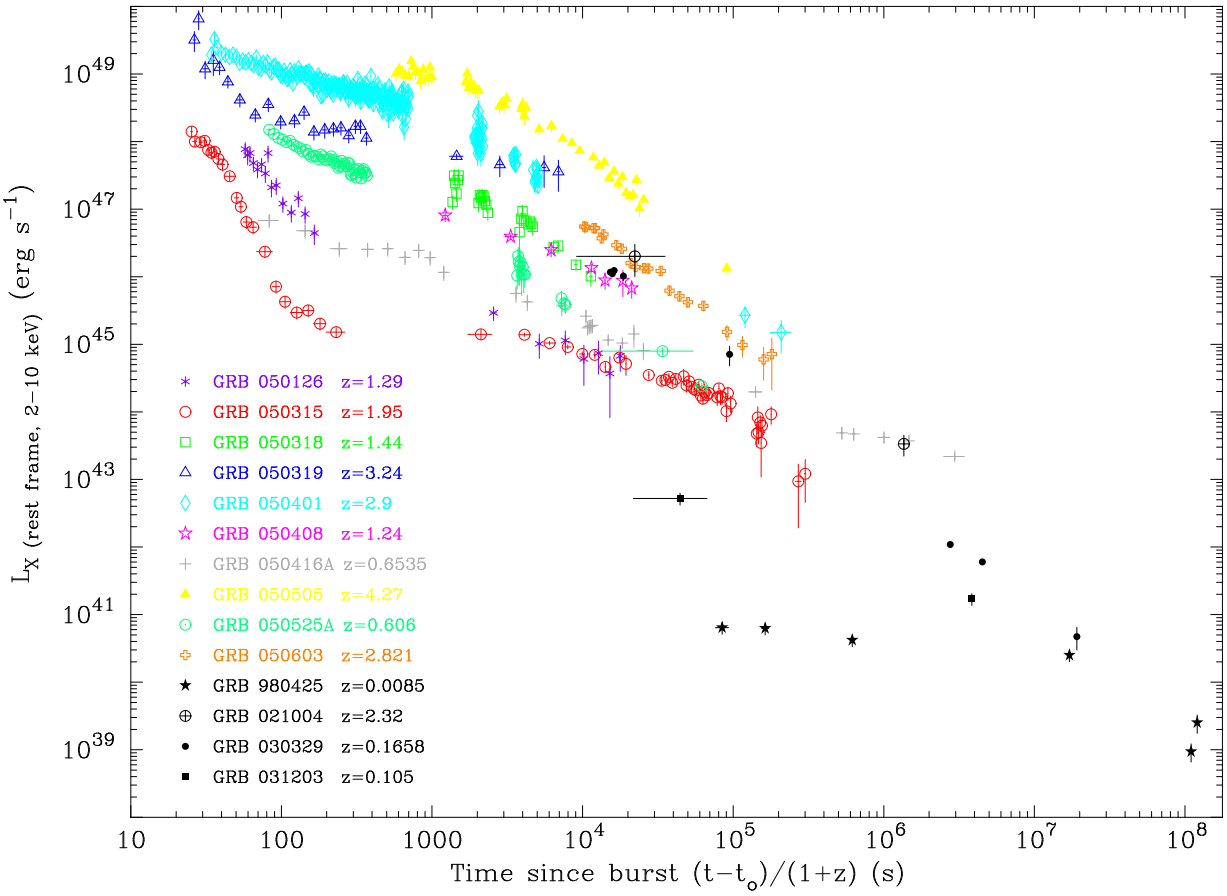

Fig. 1.— The X-ray luminosity in the range 2−10 keV as a function of time (both measured in the cosmological rest frame of the GRB) for *Swift* GRBs with established redshifts (coloured symbols), plotted together with selected earlier events (all in black symbols) from Figure 3 in Kouveliotou et al. (2004).

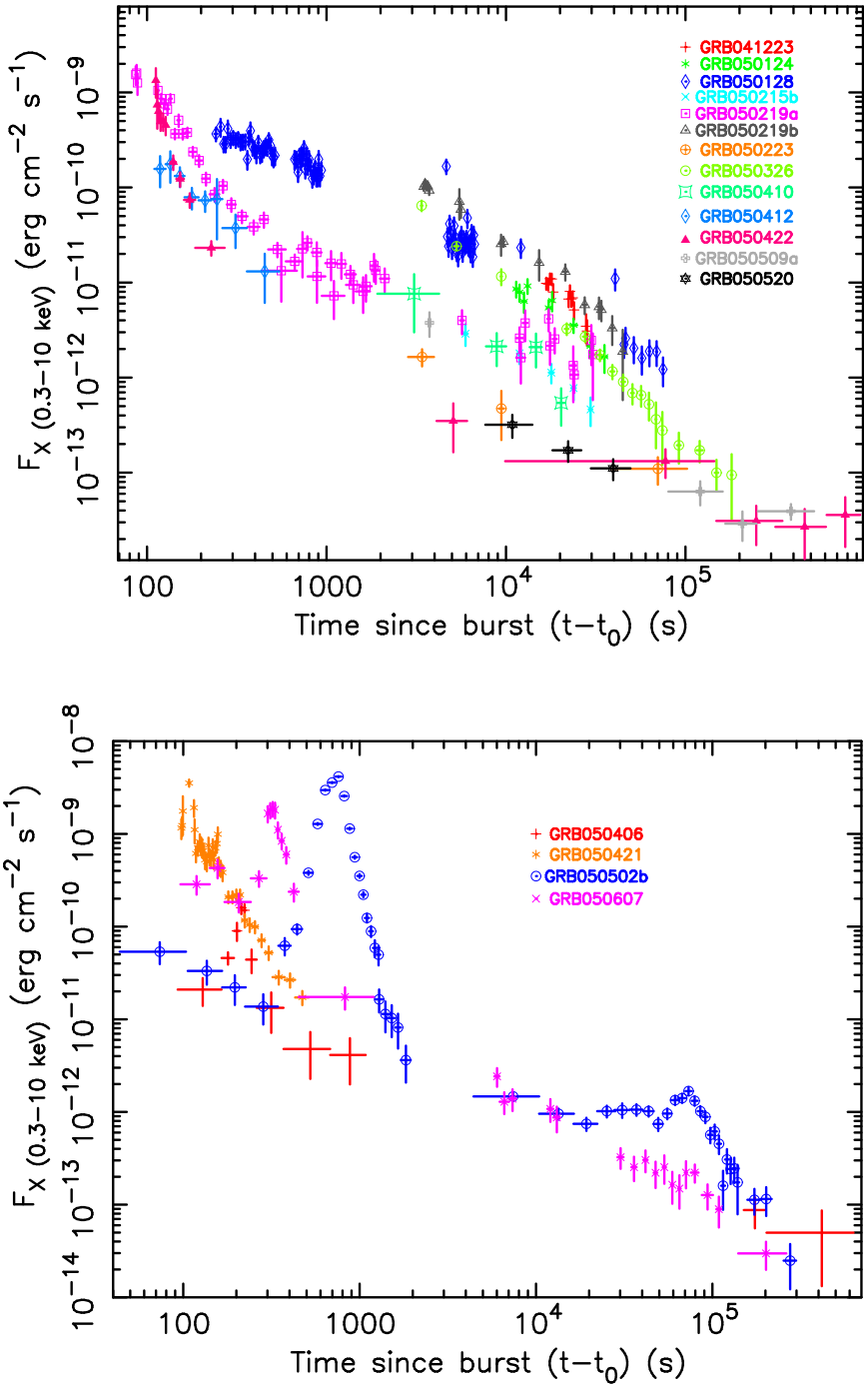

Fig. 2.— The X-ray flux ($0.3 - 10$ keV in the observer frame) as a function of the observed time, for all *Swift* GRBs without known redshifts, with (*upper panel*) and without (*lower panel*) X-ray flares.

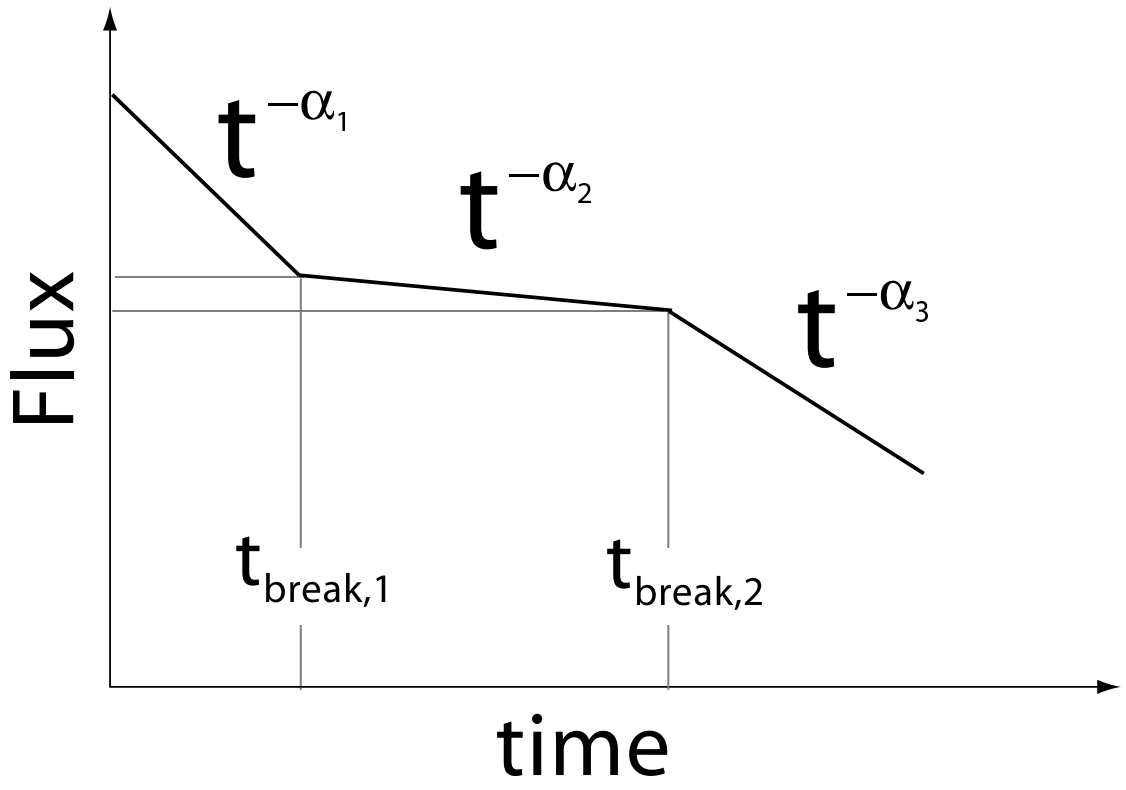

Fig. 3.— A schematic diagram of the canonical behavior of the early X-ray light curve for GRBs observed with *Swift* XRT. It consists of three power law segments where $F_\nu \propto \nu^{-\beta} t^{-\alpha}$: (i) a fast initial decay with $3 \lesssim \alpha_1 \lesssim 5$, (ii) a very shallow decay with $0.2 \lesssim \alpha_2 \lesssim 0.8$, (iii) a somewhat steeper decay with $1 \lesssim \alpha_3 \lesssim 1.5$. The transition between these power law segments occurs at two break times, $t_{\rm break,1}$ and $t_{\rm break,2}$.

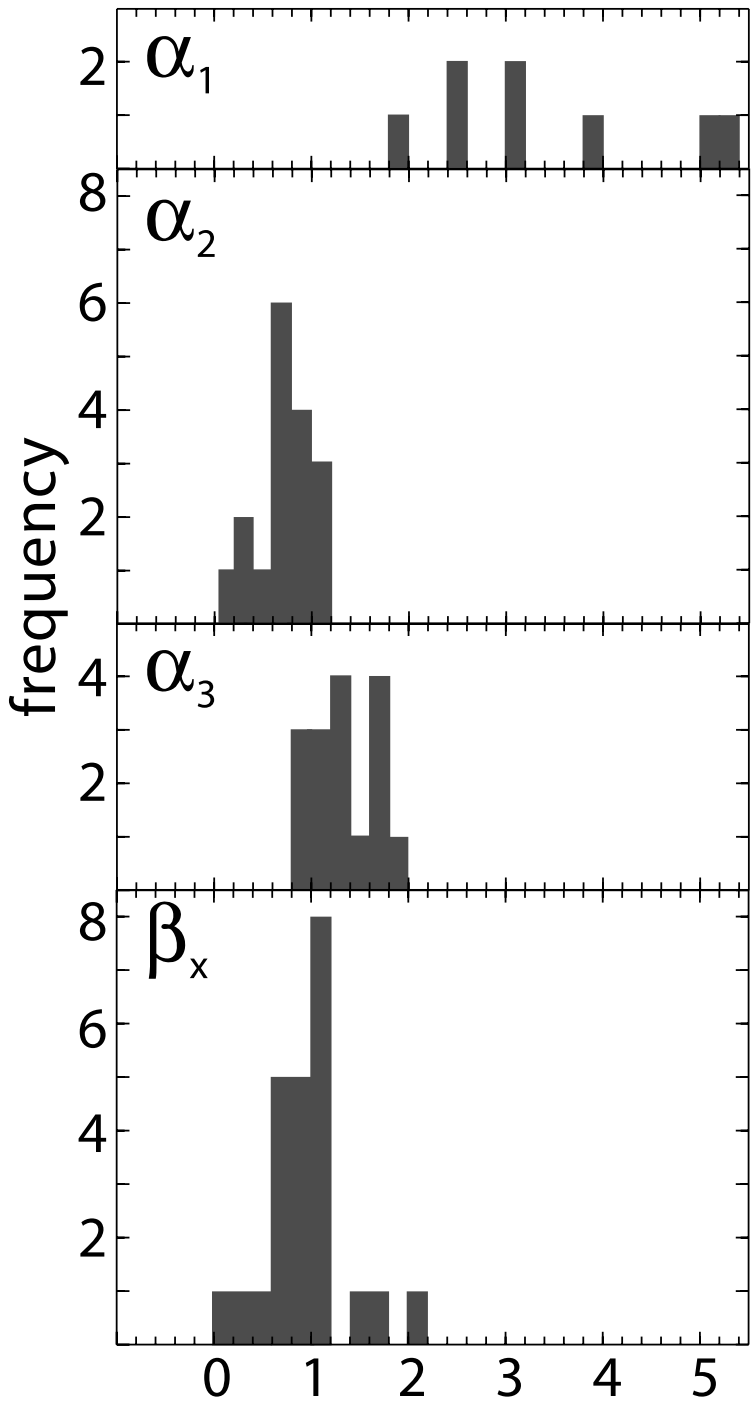

Fig. 4.— Histogram of the spectral index $\beta_{\rm x}$ and the temporal indices α_1, α_2 and α_3, for the GRBs in Table 1. Note that only $\beta_{1,\rm x}$ is plotted here for the events with evolving spectral properties. The x-scale range is the same for all indices.

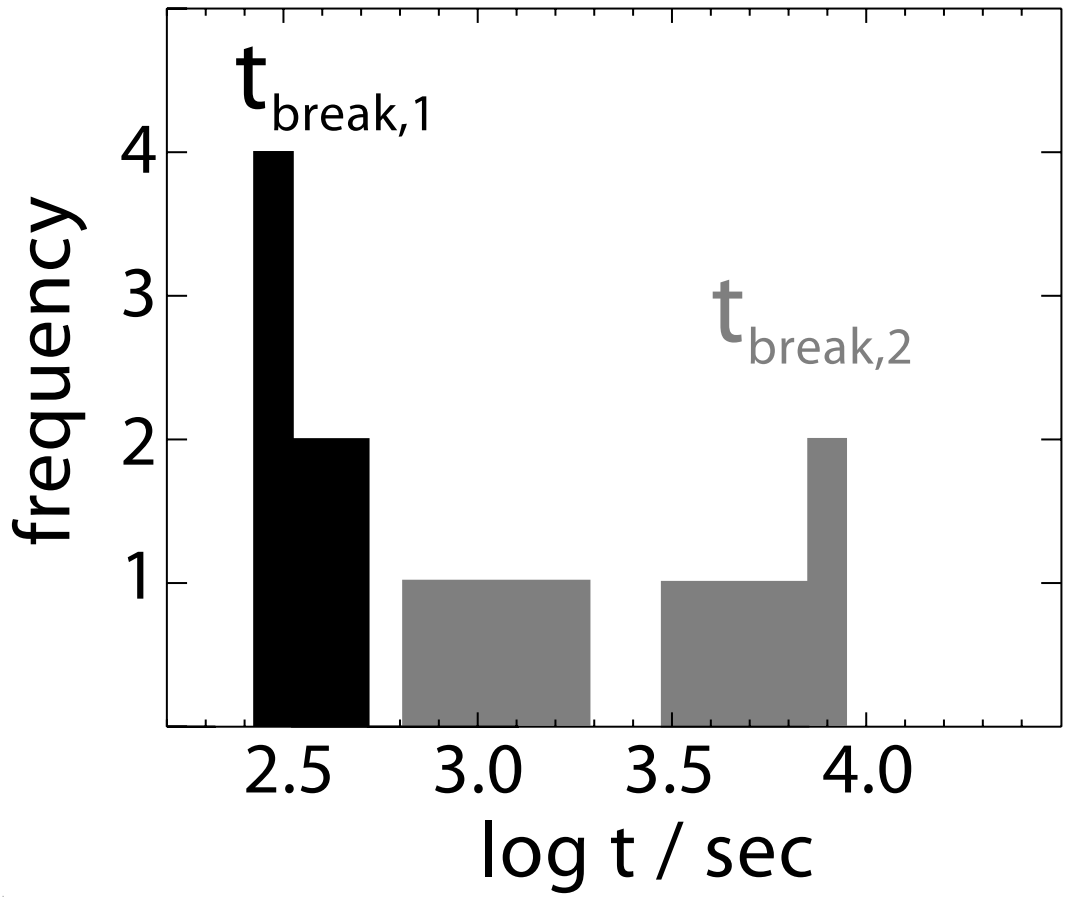

Fig. 5.— Histogram of $t_{\rm break,1}$ and $t_{\rm break,2}$.

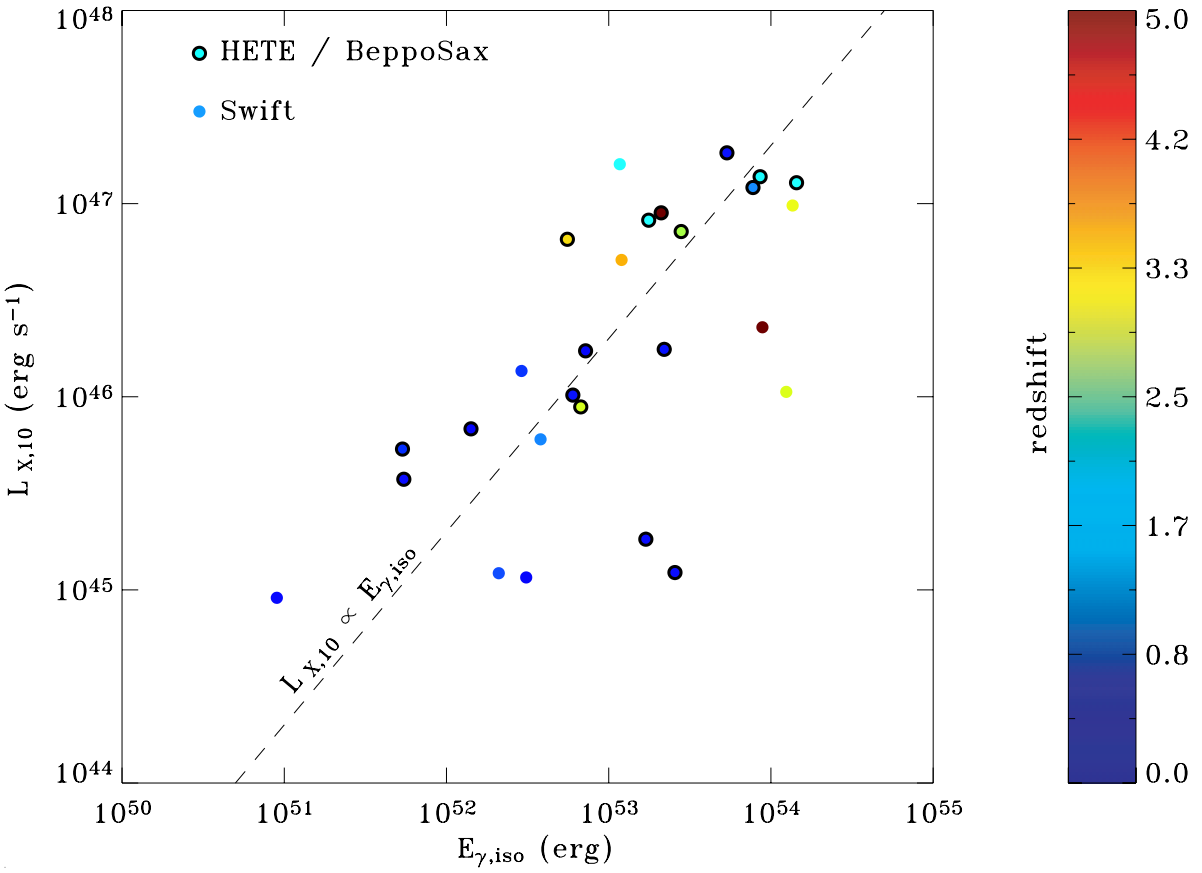

Fig. 6.— Distribution of $L_{\rm X,10}$ $(2-10$ keV) versus $E_{\gamma,\rm iso}(20-2000\,\rm keV)$ for all *Swift* GRBs with established redshifts (from Table 1) plotted together with selected earlier events observed with *HETE-II* and *BeppoSAX* (Berger et al. 2003; Bloom et al. 2003).

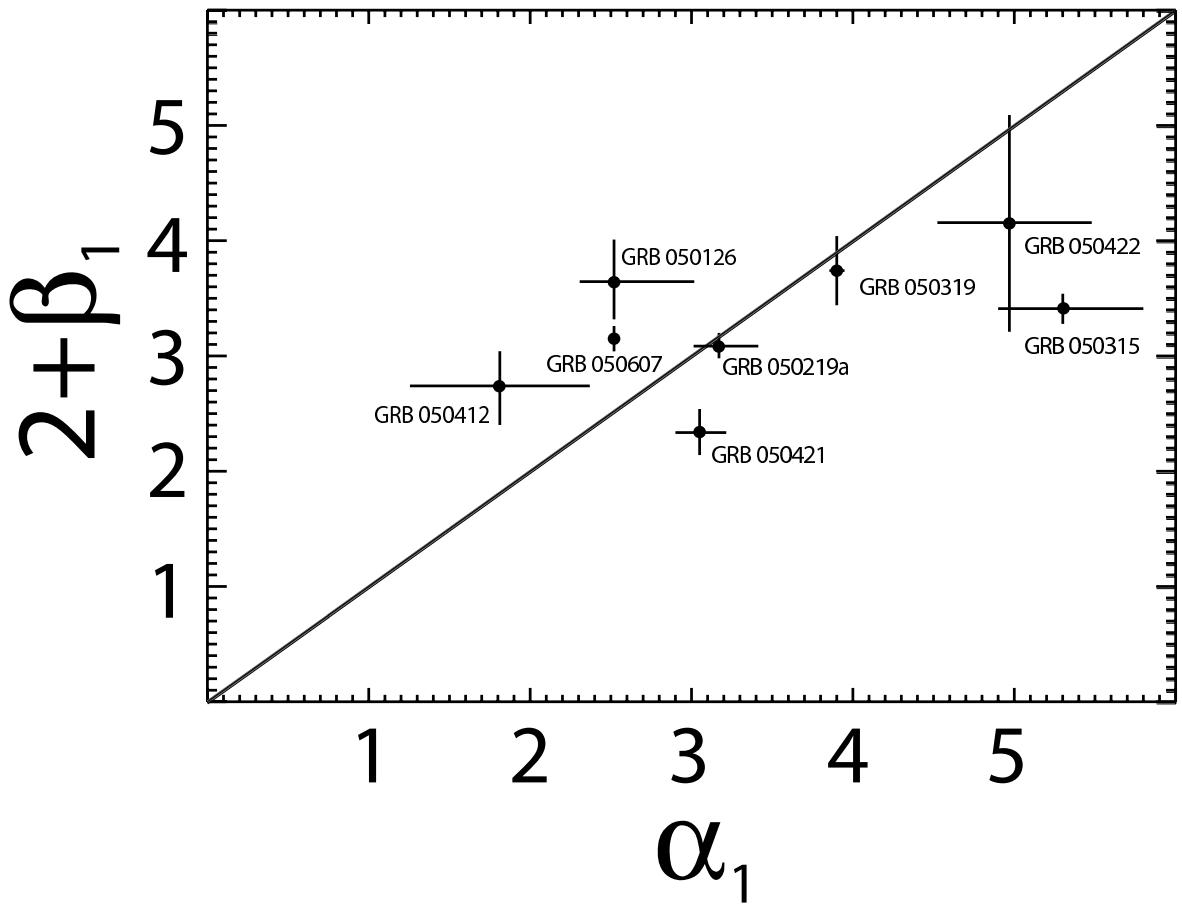

Fig. 7.— α_1 as a function of $2 + \beta_1$. The solid line gives the theoretical prediction for the prompt gamma-ray tails emitted at large angles ($\theta > \Gamma^{-1}$) relative to our line of sight (Kumar & Panaitescu 2000).

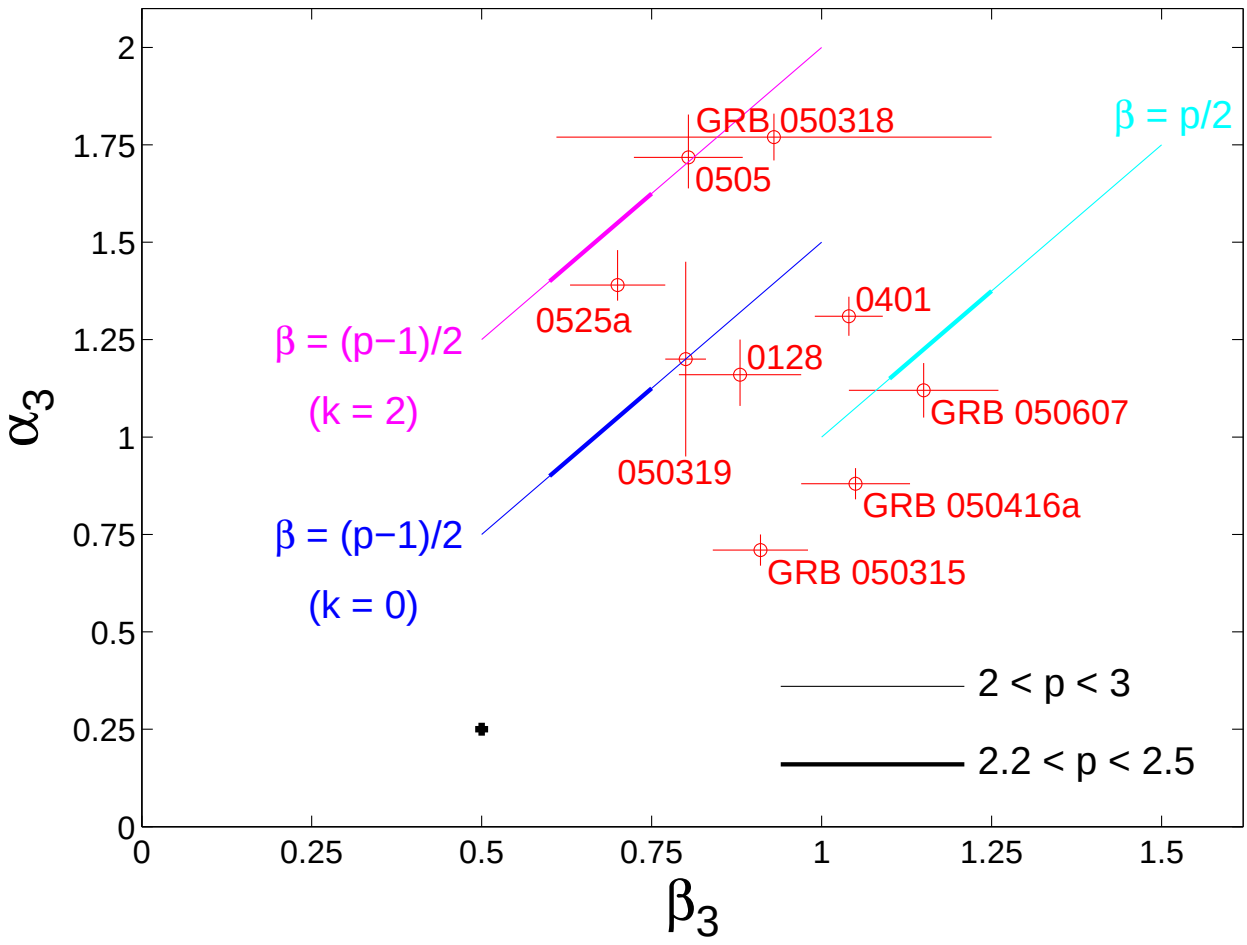

Fig. 8.— The values of α_3 and β_3 for the GRBs in our sample for which $t_{\rm break,2}$ could be determined, as well as the values expected for an adiabatic evolution of a spherical afterglow shock (Sari, Piran & Narayan 1998; Granot & Sari 2002). In most relevant power law segments of the spectrum both α and β depend on p, and therefore we drew a thick (thin) line corresponding to the range $2.2 < p < 2.5$ ($2 < p < 3$) which is both typically inferred from GRB afterglows, and is preferred on theoretical grounds. The cross at $\alpha_3 = 1/4$ and

Table 1. TEMPORAL PARAMETERS OF *Swift*/XRT GRBs

Burst	α_1	$t_{break,1}$ s	α_2	$t_{break,2}$ s	α_3	$\beta_{1,x}$ $\beta_{2,x}$	T_{burst} (SCC)[b]	XRT onset s
(1)	(2)	(3)	(4)	(5)	(6)	(7)	(8)	(9)
041223					1.72 ± 0.20	1.04 ± 0.17	125503577	16661
050124					1.58 ± 0.11	0.66 ± 0.20	128258987	11113
050126	$2.52^{+0.50}_{-0.22}$	424^{+561}_{-120}	$1.00^{+0.17}_{-0.26}$			1.64 ± 0.37	128433654	131
050128			$0.66^{+0.10}_{-0.11}$	1724^{+937}_{-565}	$1.16^{+0.09}_{-0.08}$	0.88 ± 0.09	128578795	107.7
050215B			0.75 ± 0.27			0.44 ± 0.42	130126528	> 6000
050219A	$3.17^{+0.24}_{-0.16}$	332^{+26}_{-22}	$0.75^{+0.09}_{-0.07}$			1.09 ± 0.11	130509595	92.4
050219B					1.20 ± 0.09	1.14 ± 0.09	130539888	3129
050223			$0.99^{+0.15}_{-0.12}$			0.75 ± 0.19	130820949	2874
050315	$5.3^{+0.5}_{-0.4}$	400 ± 20	$0.06^{+0.08}_{-0.13}$	12000 ± 400	0.71 ± 0.04	1.42 ± 0.12 0.91 ± 0.07[c]	132613179	83
050318			1.00 ± 0.10	10000 ± 100	1.77 ± 0.06	0.93 ± 0.32	132853476	3276.8
050319	3.9 ± 0.05	370 ± 15	0.47 ± 0.10	40000 ± 300	1.2 ± 0.25	1.74 ± 0.3 0.8 ± 0.03	132917478	87.09
050326					1.60 ± 0.06	0.80 ± 0.27	133523625	3259
050401			0.76 ± 0.02	5518^{+1149}_{-1043}	1.31 ± 0.05	1.04 ± 0.05	134058007	127
050406[e]						1.32 ± 0.15	134495928	86.6
050408					0.83 ± 0.04	1.16 ± 0.11	134670169	2547.1
050410					1.15 ± 0.10	1.05 ± 0.28	134828073	1921.6
050412	$1.81^{0.57}_{0.47}$					0.74 ± 0.32	134977437	107
050416A			0.52 ± 0.15	1350^{+2070}_{-620}	0.88 ± 0.04	1.05 ± 0.08	135342284	78.5
050421	$3.05^{+0.17}_{-0.15}$					0.34 ± 0.20	135749511	110.72
050422	$4.97^{+0.53}_{-0.37}$	272^{+43}_{-25}	$0.92^{+0.13}_{-0.16}$			2.15 ± 0.94	135849161	109.4
050502B			0.8 ± 0.2	—[d]		1.15 ± 0.02	136718724	63
050505			$0.66^{+0.13}_{-0.12}$	19889^{+5206}_{-2888}	$1.72^{+0.11}_{-0.08}$	0.804 ± 0.08	137028131	2822.2
050509A			$1.18^{+0.21}_{-0.22}$	See note[a]			137295982	> 3000
050520			$0.82^{+0.48}_{-0.52}$				138240354	7661
050525A			0.98 ± 0.05	641^{+690}_{-123}	$1.39^{+0.09}_{-0.04}$	0.70 ± 0.07	138672173	125.44
050603					1.70 ± 0.07	0.66 ± 0.07	139472941	39022
050607	2.52 ± 0.02	510 ± 50	0.61 ± 0.11	6400 ± 900	1.12 ± 0.07	1.15 ± 0.11	139828282	99

Note. — [a] Only 2 points above background; [b] The Spacecraft clock Time (SCC) is defined as 0 seconds at 01.01.2001, 00:00:00 UT; [c] GRB 050315 has a very complicated light curve; for a detailed study see Vaughan et al. (2005); the spectral indices given here correspond to the first and the third segment in the light curve, i.e., $\beta_{1,x}$ and $\beta_{3,x}$; [d] A flare event with complex structure; the temporal index is for the underlying power law decay; there is evidence for a break at $t_{break,2} \sim 10^5$ s, but is is hard to determine its exact value due to flaring activity around the same time. [e] Single flare

Table 2. Energetics of *Swift* GRBs with known redshifts

GRB #	Redshift z	Fluence[a] (10^{-6} erg/cm^2)	$E^{c*}_{\gamma,\rm iso}$ (10^{52} erg)	$E^{c**}_{\gamma,\rm iso}$ (10^{52} erg)	$L^{c}_{\rm X,1}$ (10^{45} erg/s)	$L^{c}_{\rm X,10}$ (10^{45} erg/s)
050126	1.29	1.1	0.6	2.2	14	1.2
050315	1.949	4.2	5.5	18	780	160
050318	1.44	2.1	1.3	3.9	230	6.0
050319	3.24	0.8	4.0	12.1	550	51
050401	2.90	14	42	137	1800	98
050408[b]	1.236	2.3	1.0	2.9	80	14
050416A	0.6535	0.4	0.02	0.09	5.8	0.91
050505	4.3	4.1	27	89	1100	23
050525A	0.606	20	1.6	3.1	29	1.2
050603	2.821	13	31	126	... [d]	11

Note. — [a] Fluence is calculated between $15-350$ keV; [b] HETE burst, fluence is converted from $30-400$ kev using a spectral index of $\beta=-1.979$; [c] In all conversions we assume a cosmology with $H_0=71$ km s^{-1} Mpc^{-1}, $\Lambda=0.27$ and $\Omega=0.73$; [d] XRT slewed 11 hours after trigger;* $E_{\gamma,\rm iso}$ is k-corrected and re-calculated between $100-500$ keV;** $E_{\gamma,\rm iso}$ is k-corrected and re-calculated between $20-2000$ keV

Table 3. Energetics and Microphysical Parameters of *Swift*/XRT GRB Afterglows

GRB #	T_{90}/s	$\Delta\alpha$	$\beta(p)$	k	p	b	s	q	$f_{\rm min}$	$f_{\rm max}$
050128	13.8	0.5 ± 0.1	$(p-1)/2$	0	2.6 ± 0.2	1.4 ± 0.1	2.1 ± 0.2	- 0.6 ± 0.1	2.1	5.5
050315	96.0	0.6 ± 0.1	$p/2$	0	1.7 ± 0.2	0.9 ± 0.1	3.4 ± 0.1	-0.3 ± 0.1	10.8	29.3
050318	32.0	0.8 ± 0.1	$(p-1)/2$	2	2.4 ± 0.4	0.9 ± 0.1	34.9 ± 30.9	-0.1 ± 0.1	4.2	170.4
050319	10.0	0.73 ± 0.3	$(p-1)/2$	0	2.6 ± 0.2	1.4 ± 0.1	2.6 ± 0.5	-0.5 ± 0.1	11.5	75.5
050401	33.0	0.5 ± 0.1	$p/2$	0	2.2 ± 0.1	1.0 ± 0.1	2.7 ± 0.1	-0.5 ± 0.1	5.6	14.1
050416a	2.4	0.4 ±0.1	$p/2$	0	2.0 ± 0.1	1.0 ± 0.1	2.1 ± 0.1	-0.6 ± 0.1	2.2	9.9
050505	60.0	1.1 ± 0.1	$(p-1)/2$	2	2.28 ± 0.2	0.8 ± 0.1	-16.7 ± 4.6	0.3 ± 0.1	19.4	1795.0
050525a	8.8	0.4 ± 0.1	$(p-1)/2$	2	2.0 ± 0.1	0.7 ± 0.1	5.9 ± 0.8	-0.4 ± 0.1	2.1	5.9
050607	26.5	0.5 ± 0.1	$p/2$	0	2.2 ± 0.2	1.1 ± 0.1	2.5 ± 0.1	-0.5 ± 0.1	3.4	14.1